ISSN 1063-7710, Acoustical Physics, 2010, Vol. 56, No. 4, pp. 412–421. © Pleiades Publishing, Ltd., 2010.

CLASSICAL PROBLEMS OF LINEAR ACOUSTICS AND WAVE THEORY

Propagation Characteristics of Guided Waves in a Rod Surrounded by an Infinite Solid Medium[1]

Hanyin Cui[a, b], Bixing Zhang[a], and Shunxin Ji[a]

[a] *State Key Laboratory of Acoustics, Institute of Acoustics, Chinese Academy of Sciences, Beijing 100190, People's Republic of China*

[b] *Durham University, Durham, UK*

e-mail: cuihanyin@mail.ioa.ac.cn, zhbx@mail.ioa.ac.cn

Received June 19, 2009

Abstract—The dispersion and excitation characteristics of the guided waves in a rod surrounded by an infinite solid medium (cladding) are investigated. First, the bisection technique is employed to find all the roots of the dispersion function on the basis of theoretical analysis and to obtain the complex phase and group velocity dispersion curves of the guided modes. Second, according to their different dispersion characteristics, the guided modes are divided into two categories: normal modes and Stoneley modes. And it is concluded that the normal modes merely exist in the "hard cladding" model in which the cladding's shear velocity is larger than the rod's; while the Stoneley modes in cylindrical interface are highly dispersive and merely exist in the model whose acoustical parameters satisfied the existence condition of the Stoneley waves. Third, the seldom discussed issue, the excitation mechanisms of the guided waves, excited by three source models: symmetric point source, axial and radial force sources, are simulated respectively. Attention is paid on the dominant mode which has better excitation sensitivity and the suitable excitation frequency range. Moreover, the propagation characteristics of the Stoneley modes, ignored in previous references, are analyzed and compared with those of the normal modes.

DOI: 10.1134/S1063771010040020

1. INTRODUCTION

It is an interesting research topic that guided waves propagated in a rod surrounded by an infinite solid medium. One important application of this topic is ultrasonic non-destructive testing for the rockbolts. In engineering constructions, numerous rockbolts, which are long steel rods, are inserted into the groundwork to prevent the slippage of the rock and to ensure the stability of the groundwork. There are thousands upon thousands rockbolts at the important building sites. An essential problem is how to use the elastic waves propagated in the steel rockbolt [1–4] to estimate the bonding state between the rockbolt and the surrounding rock. It gives us a good research topic.

There have been some researches on this topic. Gazis [5] investigated free harmonic waves propagated in the hollow circular cylinders both in analytical and numerical results. Pao [6, 7] developed a technique to determine the phase and group velocity dispersion curves in elastic solids and researched the dispersive flexural waves in circular cylinder. Thurston [8] studied the elastic waves' propagation in a solid rod surrounded by another solid medium. The study is mainly for the case that the medium outside the rod has finite thickness which is aimed for modeling the ultrasonic delay line memories. Rose et al. [9–11] studied the non-axisymmetric guided waves in a hollow cylinder by using the normal mode expansion method. Lowe et al. [12–15] performed systematical study about the guided waves, with circumferential orders equal to 0 and 1, in a multi-layered cylindrical elastic solid medium. Bixing Zhang et al. [16], Kawald et al. [17], and Kley et al. [18] theoretically and experimentally studied and developed the dispersion properties of the guided waves in cylindrical multi-layered media.

However, these studies were all focused on the dispersion characteristics of the guided waves without considering the excitation characteristics of the guided waves. Although it tells us the phase and group velocities of the guided waves can be determined by the dispersion equation, it dose not show that the modes can be certainly excited and received in practical situation. For a given source, the differences among the excitation amplitudes of guided waves are significant, and they depend on the waves' excitation characteristics. In many cases, we want to know which modes are dominant. However, this problem has no any answers in the previous researches about the wave propagation for the rockbolt testing. The one of the main aims of this paper is to use the mode's excitation mechanisms to locate which modes have greater amplitudes, which modes haves less amplitudes, and to find out which

[1] The article is published in the original.

modes are dominant and which modes are too small to be received. This study lays a theoretical foundation for the rockbolt testing.

On the basis of theoretical analysis and numerical simulations about the guided waves propagated along a rod surrounded by an infinite-thickness elastic solid medium (cladding), not only are the dispersion characteristics studied further, but also the excitation characteristics are investigated for the first time in this paper. First, the dispersion equation and the excitation amplitude representations are given in theory. Then, the dispersion curves of all the possible axisymmetric longitudinal modes and non-axisymmetric flexural modes are numerically obtained by using the bisection technique. Finally, the excitation intensity characteristics of the guided waves excited by the symmetric point source, the axial and radial force sources are analyzed in detail.

2. THEORY

A rod with radius a and infinite length surrounded by an infinite cladding solid medium are considered. Both the rod and cladding are isotropic elastic solids. In the rod, the velocities of P waves and S waves are V_{p1} and V_{s1}, and the density is ρ_1. In the cladding, the velocities of P waves and S waves are V_{p2}, V_{s2}, and the density is ρ_2. As depicted in Fig. 1, it is convenient to adopt cylindrical coordinates (r, θ, z) where the z-axis is along the symmetric axis of the rod. The cladding extends to infinite both along the z-axis and the radial direction (the r-axis). The excitation source is placed in the coordinate origin to excite the elastic wave. The following theoretical analysis is conducted in the frequency-wavenumber domain $(\omega - k_z)$ where ω and k_z are the angular frequency and wavenumber in the z axis.

For the displacement vector $\mathbf{U}$ in solid medium, it is usually introduced by 3 displacement potentials ϕ, ψ, and χ which denote the compressional (P), shear vertical (SV), and shear horizontal (SH) waves respectively [19–21].

$$\mathbf{U} = \nabla\phi + \nabla \times (\chi e_z) + \nabla \times \nabla \times (\psi e_z). \qquad (1)$$

It is easy to find that the displacement potentials ϕ, ψ, and χ all satisfy the Helmholtz equation. For convenient in the following, the displacement potentials are denoted by the subscripts 1 and 2 for the rod and cladding respectively.

In the rod, the displacement potentials ϕ_1, ψ_1, and χ_1 can be expressed as [19–21]

$$\begin{cases} \phi_1 = [A_1 I_n(\alpha_1 r) + B_1 K_n(\alpha_1 r)]\cos n(\theta - \theta_0), \\ \psi_1 = [C_1 I_n(\beta_1 r) + D_1 K_n(\beta_1 r)]\cos n(\theta - \theta_0), \\ \chi_1 = [E_1 I_n(\beta_1 r) + F_1 K_n(\beta_1 r)]\sin n(\theta - \theta_0), \end{cases} \qquad (2)$$

where I_n and K_n are the nth-order modified Bessel functions of the first and second kinds, respectively;

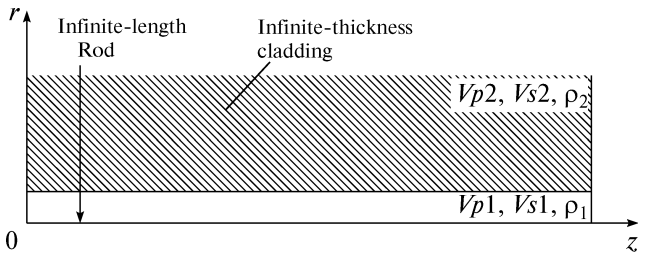

Fig. 1. Geometry of the model, which is a rod surrounded by an infinite solid cladding.

n is the circumferential order of the acoustical field which is determined by the source, and θ_0 represents the azimuth of the source. $\alpha_1 = \sqrt{k_z^2 - k_{p1}^2}$, $\beta_1 = \sqrt{k_z^2 - k_{s1}^2}$, $k_{p1} = \omega/V_{p1}$, $k_{s1} = \omega/V_{s1}$, $k_z = \omega/V$, V is the phase velocity along the rod axis. The compressional potential ϕ_1 and shear vertical potential ψ_1 are symmetrical about the plane $\theta = \theta_0$, while the shear horizontal potential χ_1 is anti-symmetrical about the plane $\theta = \theta_0$. For the axisymmetric source ($n = 0$), the potentials are not related to the angle θ and the shear horizontal potential χ_1 does not exist.

The second terms in Eq. (2) is infinite at $r = 0$ and denote the out-going waves from the origin to infinite, which is the direct field generated by the source. Then B_1, D_1, and F_1 are known coefficients for a given source. The first terms in Eq. (1) is finite at $r = 0$ and denote incoming wave from infinite to origin, which is generated by the interface between the rod and cladding and usually named as the reflection field.

In the cladding, the acoustical field tends to zero as the radial distance r increasing to infinite. Thus, the three displacement potentials ϕ_2, ψ_2, and χ_2 can be written as

$$\begin{cases} \phi_2 = B_2 K_n(\alpha_2 r)\cos n(\theta - \theta_0), \\ \psi_2 = D_2 K_n(\beta_2 r)\cos n(\theta - \theta_0), \\ \chi_2 = F_2 K_n(\beta_2 r)\sin n(\theta - \theta_0), \end{cases} \qquad (3)$$

where $\alpha_2 = \sqrt{k_z^2 - k_{p2}^2}$, $\beta_2 = \sqrt{k_z^2 - k_{s2}^2}$, $k_{p2} = \omega/V_{p2}$, $k_{s2} = \omega/V_{s2}$; B_2, D_2, and F_2 are the weighting coefficients.

Using the displacement potentials, the displacement (U) and stress ($\boldsymbol{\tau}$) in the rod and cladding can be easily obtained. At the interface of the rod and clad-

Table 1. The value of n and representations of coefficients B_1, D_1, and F_1 for the symmetric point source, axial force source, and radial force source

Source	n	B_1	D_1	F_1
Symmetric point source	0	1	0	0
Axial force source	0	ik_z	-1	0
Radial force source	1	$-\alpha_1$	$-\frac{ik_z}{2\pi\beta_1}$	$\frac{1}{2\pi\beta_1 V_{s1}^2}$

ding, displacement and stress are continuous and the boundary conditions at the interface $r = a$ are

$$\begin{cases} U_r^{(1)} = U_r^{(2)} \\ U_z^{(1)} = U_z^{(2)} \\ U_\theta^{(1)} = U_\theta^{(2)} \\ \tau_{rr}^{(1)} = \tau_{rr}^{(2)} \\ \tau_{rz}^{(1)} = \tau_{rz}^{(2)} \\ \tau_{r\theta}^{(1)} = \tau_{r\theta}^{(2)}, \end{cases} \quad (4)$$

where the superscripts (1) and (2) represent the fields inside and outside the rod, respectively. Equation (4) constitutes a linear equation group in which the number of the equations (six) is equal to that of the weighting coefficients. Therefore, all the weighting coefficients inside and outside the rod can be determined by Eq. (4).

In the case of $n = 0$, i.e., the acoustical field is excited by an axisymmetric source, and there is no *SH* wave. Thus, the displacement and stress components U_θ and $\tau_{r\theta}$ are equal to zero ($E_1 = F_1 = F_2 = 0$). Therefore, the linear equation group left four equations with four weighting coefficients.

With Eqs. (1)–(4), the representation of displacement components are obtained. For example, the radial displacement component in the rod $U_r^{(1)}$ can be written as the following form

$$U_r^{(1)}(\omega, k_z, r, \theta) = \frac{\Delta_1}{\Delta}\cos n(\theta - \theta_0), \quad (5)$$

where Δ is the coefficient determinant of Eq. (4), and Δ_1 can be obtained by applying the Cramer's formulas.

Equation (5) has many poles which can be determined by

$$\Delta = 0. \quad (6)$$

This equation is just the dispersion equation of the guided waves. Then, the excitation displacement intensities of the guided waves can be given by the residues of the poles, for example, the displacement amplitude $U_r^{(1)}$ of the guided waves can be written as

$$U_r^{(1)}(\omega, r, \theta, z) = \frac{2\pi i\Delta_1}{\Delta'} e^{ik_z z}\cos n(\theta - \theta_0)\Big|_{k_z = k_m}, \quad (7)$$

where $\Delta' = \frac{\partial\Delta}{\partial k_z}$, and k_m is the wave-number corresponding to the mth pole for a given frequency ω.

3. NUMERICAL SIMULATION

For the guided wave in the rod, because the propagation direction of the energy should be along the z-axis, it demands that the phase velocity of the guided wave less than the shear velocity of the cladding, i.e.,

$$\beta_2^2 > 0. \quad (8)$$

In this condition, the dispersion equation is always a real or imaginary function for the guided wave with a real wave-number k_z in the z-axis. Then, the bisection technique is used to search for all the roots of the dispersion equation, so that to obtain all the possible modes of the guided waves.

To investigate the excitation characteristics of the guided waves, three source models: the symmetric point source, axial force source, and radial force source models are considered. The coefficients B_1, D_1, and F_1 of the direct field radiated by the three sources [22–24] are known quantities, and they are presented in Table 1. It should be noted that the source is difficult to be modeled in practical situation, especially in the case of placing the source in the middle of the rod to excite the acoustic field. In this paper, we don't discuss the practical excitation of the source, but consider the excitation characteristics of the guided waves excited by these sources in theory.

The Meitzler's notation [25] for expressions of the guided waves is followed. For the guided waves excited by the three sources of this paper, the modes in the case of $n = 0$, here n is the order of acoustic field and the circumferential order, correspond to the axisymmetric longitudinal modes $L(0, m)$; and the case of $n = 1, 2, 3, \ldots$, correspond to non-axisymmetric flexural modes $F(n, m)$ with the mode order $m = 1, 2, 3, \ldots$.

Although the dispersion curves of the guided modes are independent on the source, different source types can excite different modes. The axisymmetric longitudinal modes $L(0, m)$ can be excited by axisymmetric sources (symmetric point source and axial force source). The non-axisymmetric flexural modes $F(1, m)$ can be excited by non-axisymmetric (radial force) source.

Four medium models for infinite-thickness cladding rod are chosen for numerical simulations, and their material properties are presented in Table 2. They can be sorted into two categories by their shear velocities. One category is "hard cladding model" that shear

Table 2. Material properties used to model infinite-thickness cladding rods

Model	Category	*P*-wave velocity V_P, m/s	*S*-wave velocity V_S, m/s	Density, kg/m^3	Radius, m
1	Rod	5500	3100	7800	r_1 0.01
	Hard cladding	6100	3250	2700	r_2 ∞
2	Rod	4100	2100	7800	r_1 0.01
	Hard cladding	5370	3100	2700	r_2 ∞
3	Rod	5500	3100	7800	r_1 0.01
	Soft cladding	5000	3050	2700	r_2 ∞
4	Rod	5500	3100	2200	r_1 0.01
	Soft cladding	5000	2500	2500	r_2 ∞

velocity of the cladding is larger than that of the rod, that is to say, $V_{s2} > V_{s1}$. The other category is "soft cladding model" that holds the relation of $V_{s2} < V_{s1}$. In the examples of this paper, models 1 and 2 belong to the hard cladding models, and models 3 and 4 belong to the soft cladding models.

The four models can also be classified into other two categories by whether their material combinations allow or not allow the Stoneley wave exist. The Stoneley wave will not exist in a planar interface of two elastic solid half-spaces until the acoustical parameters of two half-spaces meet the strict existence condition [26, 27]. While we find that for the model which is a rod surrounded by the infinite cladding, such existence condition of the Stoneley wave is still held. According to this existence condition, the material combinations of models 1 and 3 allow Stoneley waves exist, while those of models 2 and 4 don't allow.

It is divided into two sections in the following. First, the displacement spectra and dispersion curves are studied together to get primary comprehensions for the dispersion and excitation mechanisms of different modes, so that we can find out the dominant modes which hold the relatively larger displacement amplitudes and the suitable excitation frequency range. Second, the vibration distributions of the Stoneley modes and normal modes are investigated and summarized.

Moreover, we also did the comparisons to prove the numerical results presented in this manuscript are correct. For example, when the material properties of the infinite cladding rod model are $V_{S1} = 2950$ m/s, $V_{P1} = 5200$ m/s, $\rho_1 = 19200$ kg/m^3, $V_{S2} = 3180$ m/s, $V_{P2} = 4800$ m/s, and $\rho_2 = 2845.3$ kg/m^3, which are the same as those of the example used in Fig. 24 in page 23 of the literature [8], the numerical results of dispersion curves calculated by our program are same as those in the Fig. 24. For the paper length limit, the calculated dispersion curves are not shown in this paper.

3.1. Dispersion Curves and Excitation Displacement Spectra

In order to analyze the dispersion and excitation characteristics in a straight forward view, the phase and group velocities dispersion curves are all illustrated along with their corresponding displacement curves. And for convenience, all the displacement curves in this paper are normalized against the value, which is slightly larger than the maximum value of the displacement amplitude, to keep the range of displacement variation between 0 and 1. Similarly, all the dispersion curves are also normalized against the shear velocity of the rod V_{s1}.

The propagation characteristics of the guided waves are studied according to the hard and soft claddings. First, the results of the hard cladding models 1 and 2 are presented. Then, those of the soft cladding models 3 and 4 are analyzed.

3.1.1. Hard cladding models, $V_{s2} > V_{s1}$. Models 1 and 2 belong to this case. The material combination of model 1 satisfies the existence condition of Stoneley wave, while that of model 2 does not.

(a) Model 1

Figures 2a and 2b present the dispersion curves of $L(0, m)$ ($m = 1, 2, ..., 6$) and $F(1, m)$ ($m = 1, 2, ..., 11$) modes in model 1. Moreover, the displacement spectra of the $L(0, 1)$ and $L(0, m)$ ($m = 2, 3, ..., 6$) modes, excited by the symmetric point source, with the radial distance $r = 10$ mm are shown in the left and right vertical axes of Fig. 2c, respectively; and those of the $F(1, 1)$ and $F(1, m)$ ($m = 2, 3$) modes excited by the radial force source are shown in the left and right vertical axes of Fig. 2d, respectively. In Figs. 2a and 2b, the solid, dashed, and dotted lines represent the phase and group velocity dispersion curves, and the V_{s1} and V_{s2}, respectively. And, in Figs. 2c and 2d, the solid and dashed lines represent the radial and axial direction displacement components, which are denoted as U_r and U_z for short, respectively.

As shown in Figs. 2a and 2b, the guided waves in model 1 can be classified into two categories by their high-frequency velocity asymptotes. The first category

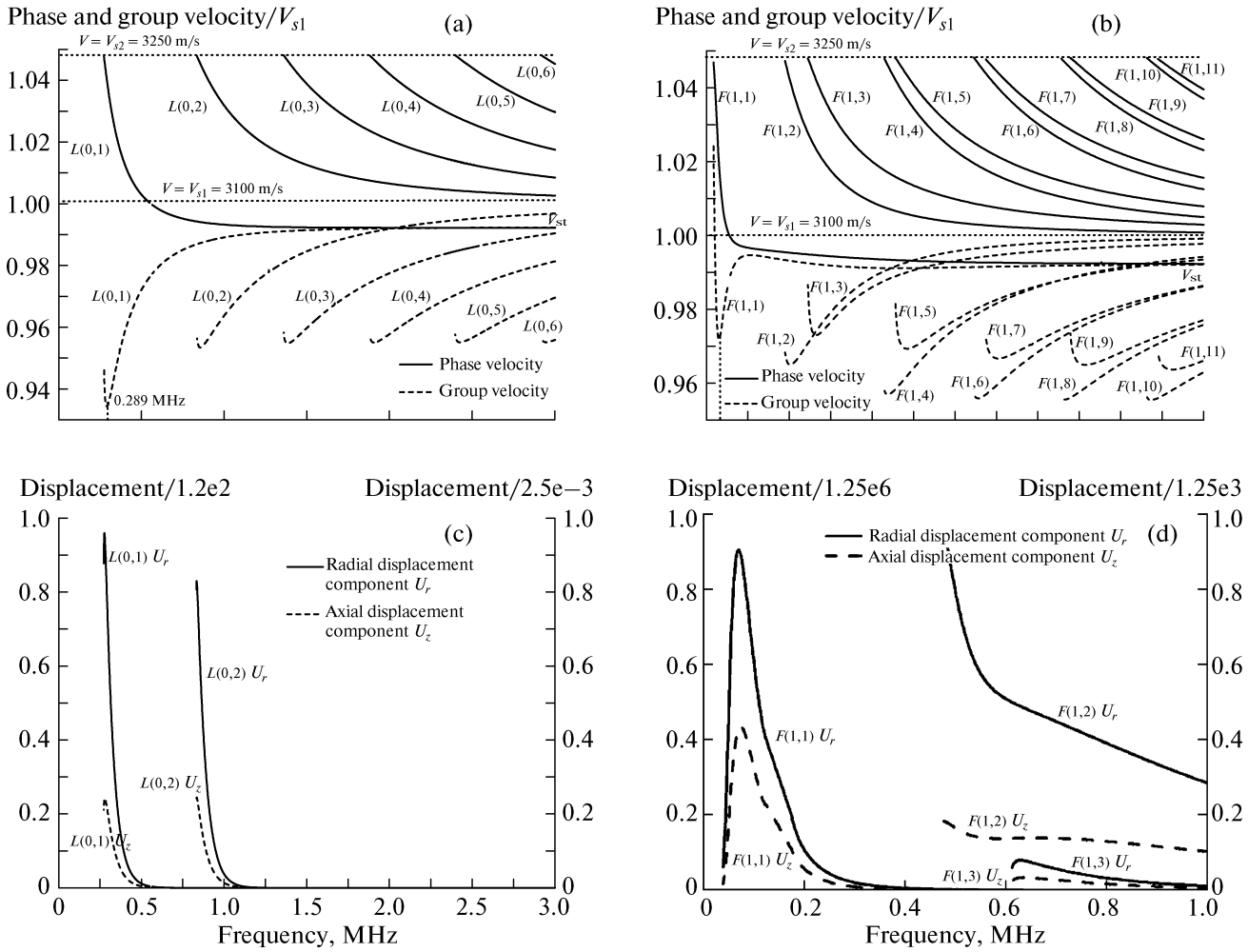

Fig. 2. In model 1, the phase and group velocity dispersion curves of the (a) $L(0, m)$ ($m = 1, 2, ..., 6$) and (b) $F(1, m)$ ($m = 1, 2, ..., 11$) modes, in 0–3 MHz; the displacement spectra of (c) the Stoneley mode $L(0, 1)$ in the left coordinate and the normal modes $L(0, m)$ ($m = 2, 3, ..., 6$) in the right coordinate, excited by the symmetric point source in 0–3 MHz; and (d) the Stoneley mode $F(1, 1)$ in the left coordinate and the normal modes $F(1, m)$ ($m = 2, 3$) in the right coordinate, excited by the radial force source in 0–1 MHz, at the radial distance $r = 10$ mm.

is the lowest order modes ($m = 1$) whose phase and group velocities in the high-frequency range tend to the velocity of the Stoneley wave (V_{st}). This Stoneley wave is the wave propagating in the interface of two half-infinite solid spaces which has the same acoustic parameters of the rod and the cladding of model 1. This category of the modes is named as the Stoneley modes in the cylindrical interface. In contrast with the non-dispersive Stoneley waves in planar interface, these Stoneley waves in cylindrical interface are highly dispersive. Their phase and group velocity dispersion curves start from their cutoff frequency, vary with the increasing frequency, and finally end at high frequency with the asymptote V_{st} that is smaller than the smaller one between the shear velocities of the rod and the cladding (V_{ss}). For instance, the modes $L(0, 1)$ in Fig. 2a and $F(1, 1)$ in Fig. 2b are the Stoneley modes in this case. The cutoff frequencies of the modes $L(0, 1)$ and $F(1, 1)$ are nonzero and zero (respectively) at which the phase velocities are both the V_{s2} (the shear velocity of the cladding). Their high frequency velocity asymptote is the Stoneley velocity (here V_{st} is about 3077 m/s), which is below the dotted line represents the smaller shear velocity $V_{ss} = V_{s1} = 3100$ m/s (the shear velocity of the rod).

The second category can be named as the "normal modes" of which phase and group velocities in the high frequency range tend to the V_{ss}. Here, the V_{ss} is the shear velocity of rod ($V_{ss} = V_{s1} = 3100$ m/s), and it is higher than the Stoneley velocity. For instance, the modes $L(0, m)$ ($m > 1$) in Fig. 2a and $F(1, m)$ ($m > 1$) in Fig. 2b belong to the normal modes, and they have nonzero cutoff frequencies at which the phase velocity is V_{s2}.

From the dispersion curves, we can obtain that there is infinite guided modes probably exist. However,

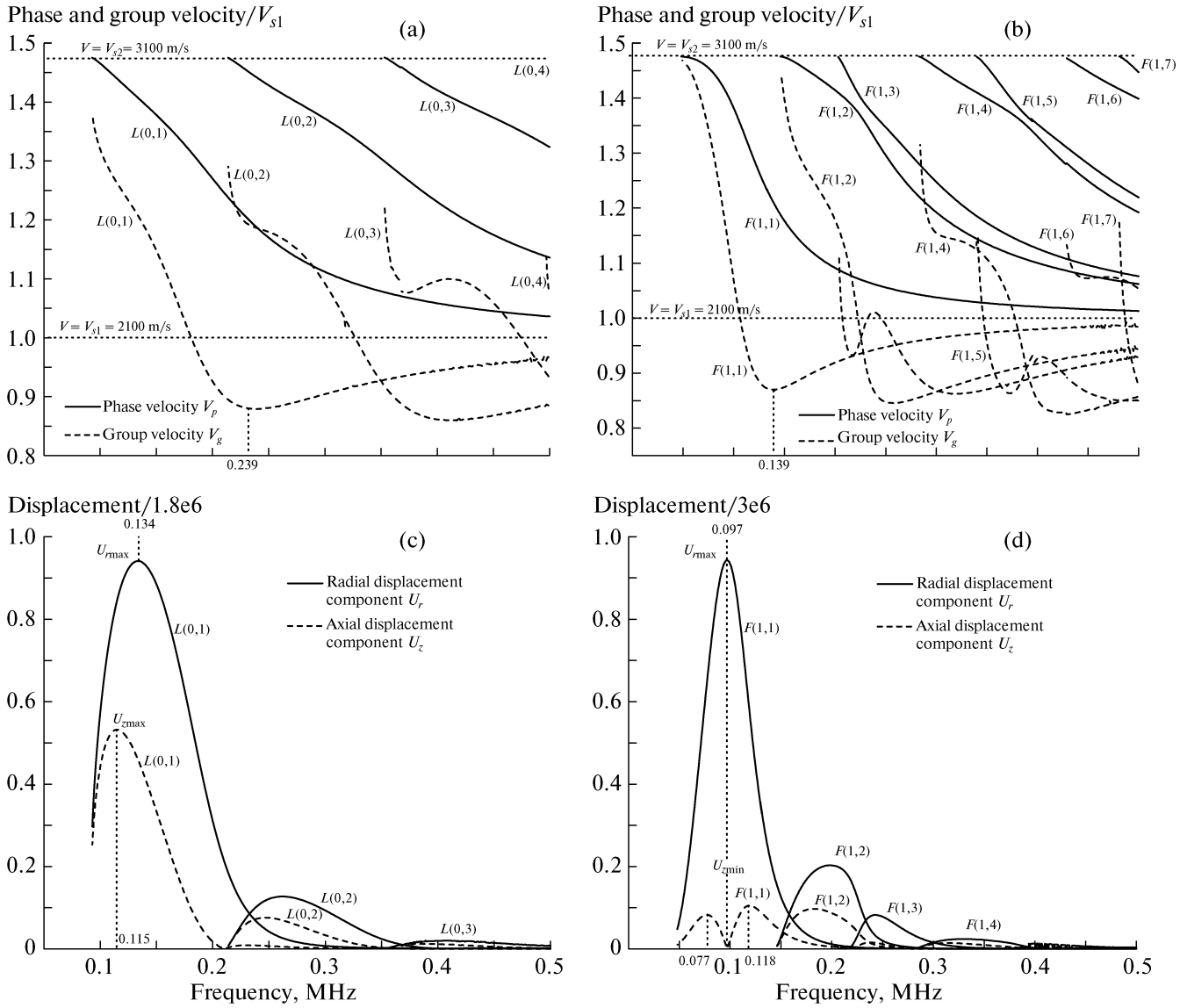

Fig. 3. In model 2, in 0–0.5 MHz, the phase and group velocity dispersion curves of the normal modes (a) $L(0, m)$ ($m = 1, 2, 3, 4$) and (b) $F(1, m)$ ($m = 1, 2, ..., 7$); the displacement spectra of (c) the $L(0, m)$ ($m = 1, 2, 3, 4$) modes excited by the axial force source, and (d) $F(1, m)$ ($m = 1, 2, ..., 7$) modes excited by the radial force source, at $r = 10$ mm.

for a given source, only one or few of them is/are dominant and can be excited and received. While which modes are the domait modes? This problem is discussed by analyzing the excitation characteristics in the following.

As shown in Figs. 2c and 2d, the displacement amplitudes of the Stoneley mode $L(0, 1)$ or $F(1, 1)$ at the interface is extraordinarily larger than those of the other normal modes $L(0, m)$ or $F(1, m)$ ($m > 1$), respectively. Specially, at any radial distance, the Stoneley mode always hold the better excitation sensitivity than the normal mode in model 1. The normal modes are impossible to be seen in full-waveforms because they are seriously covered by the Stoneley mode. In model 1, there is an important fact that the guided waves received in actual measurement are the Stoneley waves instead of the normal waves.

Furthermore, we can obtain the suitable excitation frequency range from the displacement spectrum. As shown in Figs. 2c and 2d, the displacement amplitudes strongly depend on frequency. Each component receives its maximum amplitude at the frequency near where the mode reaches its minimum group velocity (V_{gmin}). For example, in Fig. 2c, U_r and U_z of the $L(0, 1)$ mode reach their maximums at 0.276 and 0.279 MHz (respectively), which are close to 0.289 MHz where is the mode's V_{gmin}. This property is useful for determination of the suitable excitation frequency range. To effectively excite one guided mode, the frequency

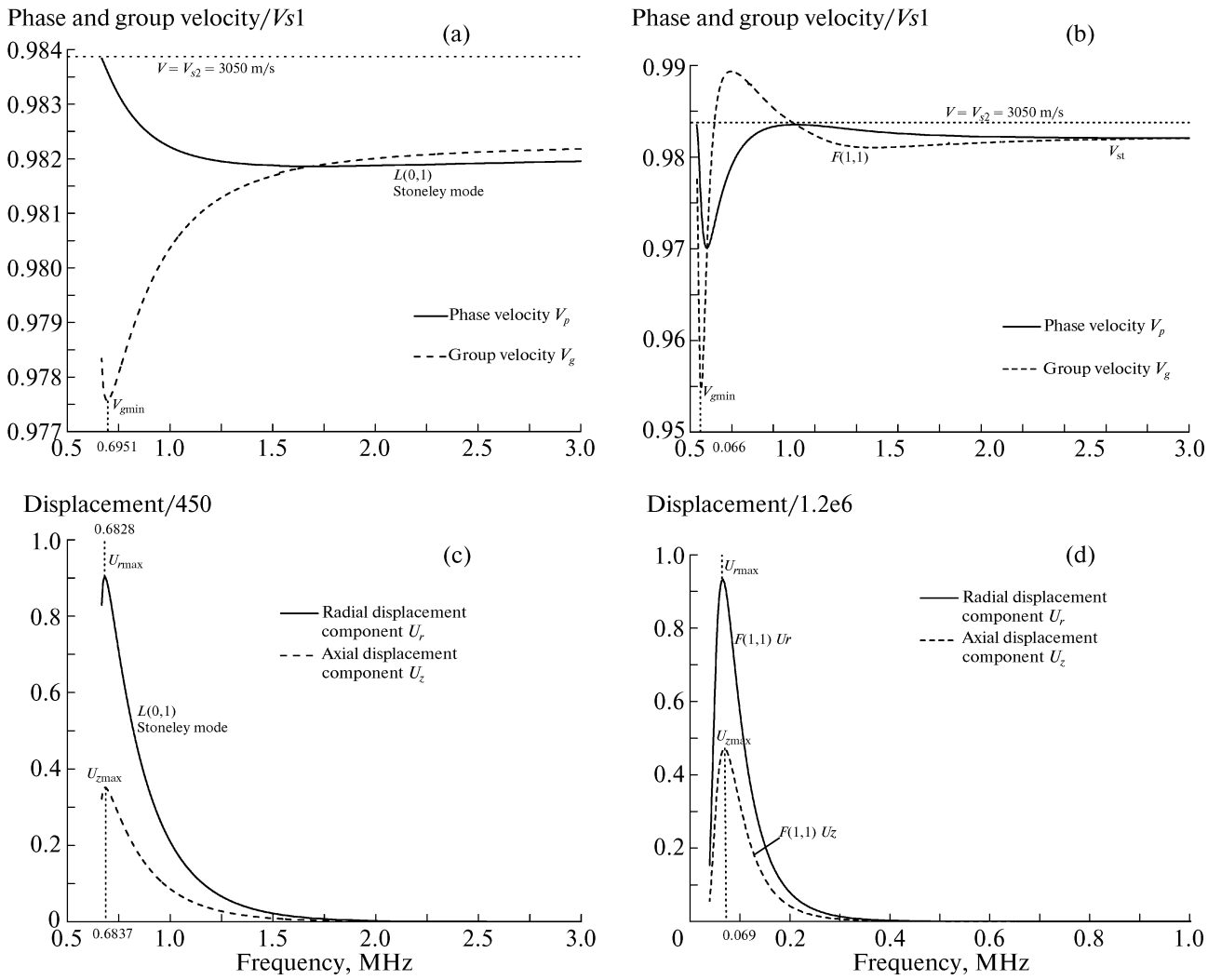

Fig. 4. In model 3, the phase and group velocity dispersion curves of the Stoneley modes (a) $L(0, 1)$ and (b) $F(1, 1)$ in 0–3 MHz; and the displacement spectra of the Stoneley modes (c) $L(0, 1)$ excited by the axial force source in 0–3 MHz, and (d) $F(1, 1)$ excited by the radial force source in 0–1 MHz.

band should be taken nearby the frequency where this mode reaches its V_{gmin}.

(b) Model 2

Model 2 also belongs to the hard cladding case and its material combination does not allow the Stoneley wave exist. The dispersion curves of both $L(0, m)$ (m = 1, 2, 3, 4) and $F(1, m)$ (m = 1, 2, ..., 7) modes are presented in Figs. 3a and 3b, respectively. And the displacement spectra of the corresponding modes, $L(0, m)$ (m = 1, 2, 3, 4) modes excited by the axial force source and $F(1, m)$ (m = 1, 2, ..., 7) modes excited by the radial force source, with r = 10 mm are shown in Figs. 3c and 3d, respectively.

In the hard cladding model 2, there are infinite guided modes which are the normal modes. As seen from Figs. 3a and 3b, the phase velocity dispersion curves start at their cutoff frequencies with the same value which is the shear velocity of the cladding, and decrease with the increasing frequency; yet the variation tendencies of the group velocity dispersion curves are so complex that the curves intersect with each other. While all the curves are asymptotic to the dotted line that represents the V_{ss}, which is the shear velocity of the rod at high-frequency.

As seen from Figs. 3c and 3d, in model 2, the dominant modes no longer limit to the lowest order modes but also include the higher order modes. For instance, as shown in Fig. 3c, the ratio of the maximum displacement amplitude of the $L(0, 2)$ mode to that of the $L(0, 1)$ mode in model 2 is above 20%. And as shown in Fig. 2c, this ratio is much smaller, below 0.02%, in model 1. Thus, both the $L(0, 1)$ and $L(0, 2)$ modes are the dominant longitudinal modes in model 2. And as shown in Fig. 3d, the $F(1, 1)$, $F(1, 2)$, and $F(1, 3)$ modes are the dominant flexural modes. Also in Fig. 3d, the displacement curves of U_z of the $F(1, 1)$

and $F(1, 3)$ modes, which have two peaks, are more irregular.

Therefore, in model 2, not only the lowest order modes but also the former higher order modes could be excited, and these normal modes have much more complicated variation relations between excitation displacement and frequency.

3.1.2. Soft cladding models, $V_{s2} < V_{s1}$. Models 3 and 4 belong to this case. Model 3 satisfies the existence condition of the Stoneley wave, while model 4 does not. And it is found that no normal mode could be excited in the soft cladding models by numerical simulation.

(a) Model 3

In Figs. 4a and 4b, dispersion curves of the $L(0, 1)$ and F(1, 1) modes are presented. And displacement spectra are shown in Figs. 4c and 4d.

As shown in Figs. 4a and 4b, only the mode $L(0, 1)$ or $F(1, 1)$ exist and are highly dispersive in the cylindrical interface of model 3. For instance, the high-frequency velocity asymptote of the Stoneley mode $L(0, 1)$ in Fig. 4a is the V_{st} (here is about 3044 m/s), which is below the smaller shear velocity $V_{ss} = V_{s2} = 3050$ m/s.

In model 3, the dominant mode is the Stoneley mode. And as shown in Figs. 4c and 4d, the variation relationships between the displacement amplitudes and frequency is relatively simple. And the suitable excitation frequency range corresponds to the frequency neighborhood where one mode receives relatively larger intensities. For instance, the suitable excitation frequency range of the $F(1, 1)$ mode in Fig. 4d is in 0.03–0.12 MHz which includes 0.066 MHz corresponding to the maximum U_r and the V_{gmin}.

(b) Model 4

Because the material combination of model 4 does not satisfy the existence condition of the Stoneley wave, and model 4 belongs to the soft cladding model, no guided modes can be found in model 4.

From above analysis, the displacement components of all the guided modes highly depend on frequency. The displacement curve starts from the mode's cutoff frequency and end at infinity with the same high-frequency asymptote zero. Moreover, the suitable excitation frequency range of the guided mode is in the neighborhood of the frequency where this mode reaches its minimum group velocity (V_{gmin}). As each mode receives its maximum displacement at the point of frequency near where this mode reaches its V_{gmin}.

In the following section, we investigated the vibration distributions of both the normal modes and the Stoneley modes on the radial cross section.

3.2. Vibration Distributions on the Radial Cross Section

Taking model 1 for example, variation relations of the U_r and U_z of both the Stoneley modes and the nor-

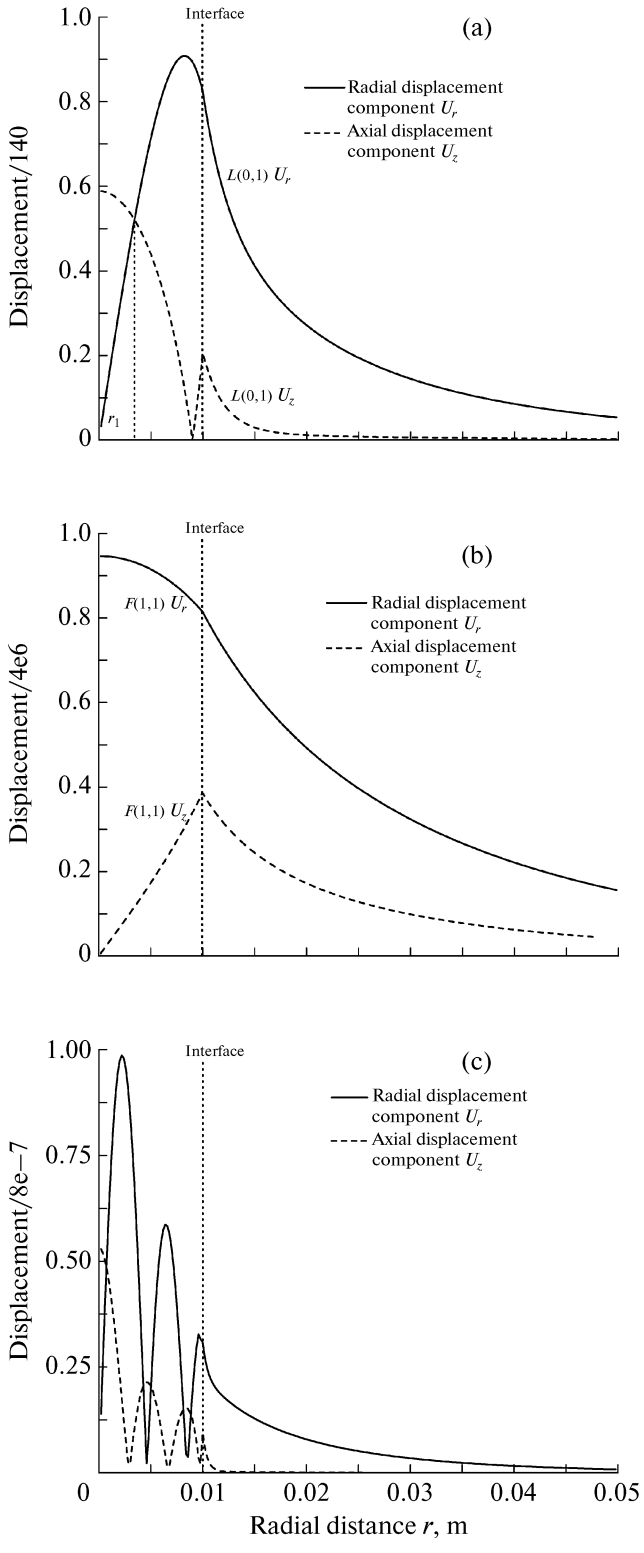

Fig. 5. In model 1, variation curves of U_r and U_z of the dominant modes with increasing radial distance r from 0.2 to 50 mm: (a) those of the Stoneley mode $L(0, 1)$ excited by the symmetric point source at 0.276 MHz; (b) those of the Stoneley mode $F(1, 1)$ excited by the radial force source at 0.066 MHz; (c) those of the normal mode $L(0, 2)$ excited by the symmetric point source at 0.834 MHz.

mal modes versus the radial distance r are analyzed. The r varies with a constant increased interval $\Delta r = 0.2$ mm from the origin through the interface $r = 10$ mm to the infinite.

Figures 5a, 5b, and 5c presents the vibration distributions of U_r and U_z of the $L(0, 1)$ mode excited by the symmetric point source at 0.276 MHz, the $F(1, 1)$ mode excited at 0.066 MHz, and the $L(0, 2)$ mode excited by the symmetric point source at 0.834 MHz. The solid, dashed, and dotted lines represent variation curves of U_r and U_z, and the interface that $r = 10$ mm.

As shown in Fig. 5a, the displacement component amplitudes of the Stoneley mode $L(0, 1)$ highly depend on the r varied from the rod centre to the receiver. At origin ($r = 0$), U_r is zero, and U_z is at its maximum. In the rod, with increasing r, variation curve of U_r first increases to the maximum peak and then decreases slightly at the point near the interface, while that of U_z first decreases to a local minimum then bounces back slightly. These curves are not monotone, as the displacement potentials of the $L(0, 1)$ mode in the rod are the linear combination of the nth-order modified Bessel functions I_n and K_n, as shown in Eq. (1). Furthermore, two curves intersect at the point denoted as "r_1" in Fig. 5a. U_z is larger than U_r before the intersection r_1, and then varies to be the smaller one when r is larger than r_1. Special attention is given to the case that guided wave propagates in the cladding. When r keeps increasing and passes the interface which is represented as the dotted line in Fig. 5a, variation curves of U_r and U_z both keep monotonously declining to zero when r tends to infinite.

From Fig. 5b, the displacement components of the Stoneley mode $F(1, 1)$ highly depend on r, too. However, for each $F(1, 1)$ mode, U_r is always larger than U_z at the same r along the whole cross section, i.e. there is no intersection of the solid and dashed curves. At origin, U_r is at its maximum, and U_z is equal to zero. In the inner layer, curve of U_r decreases slightly with the increasing r, yet curve of U_z increases and reaches its maximum at the interface. While r crosses through the interface and keeps increasing, both curves of U_r and U_z keep declining sharply to zero at infinity.

As shown in Fig. 5c, the vibration distribution of the normal mode $L(0, 2)$ are different from those of the Stoneley modes. First, the variation relations between the displacement components and r of the normal mode $L(0, 2)$ are much more complex than those of the Stoneley mode $L(0, 1)$. Second, the mode obtains its maximum displacement amplitudes in the inner layer, and it looks like the energies of the $L(0, 2)$ mode are trapped in the inner layer. In model 1, the inner layer holds the smaller shear velocity. Moreover, after analyzed numerous vibration distributions of the other normal modes in model 1, we found that most of the normal modes also obtained their maximum amplitudes in the inner layer.

Consequently, the Stoneley waves $L(0, 1)$ and $F(1, 1)$ are the interfacial waves propagated along the cylindrical interface between the rod and the infinite cladding in model 1. Their displacement amplitudes obtain their maximum near the interface, and are monotonously decaying when the radial distance r is far from the interface into the cladding, finally approaching to zero at infinity. While the normal waves have the "energy-trapped" trend. It looks like their maximum displacement amplitudes are trapped in the layer which has the smallest shear velocity.

Generally, the unitary pictures of displacement contributions of the guided modes on the radial direction cross section depend on the properties of the different excitation sources. In the case of $L(0, 1)$ mode excited by either the symmetric point source or the axial force source, U_r is zero at origin, and U_z is nontrivial. In the rod, variation curve of U_r rises with the increasing r, yet curve of U_z may drop or rise; and two curves have intersection. In the cladding, U_r is always larger than U_z at the same r.

While in the case of the $F(1, 1)$ mode excited by the radial force source, U_r is nontrivial at origin, and U_z is zero. Moreover, there is no intersection between the radial and axial curves, which means that U_r of $F(1, 1)$ mode is always larger than U_z at the same radial distance through the whole radial direction cross section. Furthermore, the variation curves of all the guided modes tend to zero at infinity, because there is no acoustic field.

5. CONCLUSIONS

The stability and robustness of numerical calculation for numerous dispersion curves are ensured by employing the bisection technique to the calculation of the complex dispersion function. And then, the essential dispersion characteristics of the guided waves propagated in the models, which material combinations allow or not allow the Stoneley waves exist, are investigated. It is found that all the modes have their high-frequency velocity asymptotes. For the Stoneley modes, their velocity asymptotes are the Stoneley wave velocity. For the normal modes, those are the smaller one between the rod's and the cladding' shear velocities. It is also found that no normal mode exists in the soft cladding model whose rod's shear velocity is larger than the cladding's.

The excitation sensitivities of the guided waves highly depend on the frequency. The displacement amplitude of each mode receives its maximum in a frequency range including the frequency where this mode's group velocity reaches its minimum. Hence, it is appropriate to set the source excitation frequency to a proper range to excite modes with stronger signal intensities. Moreover, the dominant modes are distinguished in different models. For the models which material combinations satisfy the existence condition of Stoneley wave, only the lowest branch is the domi-

nant mode, which is to say, either the Stoneley mode $L(0, 1)$ excited by the symmetric point source or axial force source, or the Stoneley mode $F(1, 1)$ excited by the radial force source, can be excited. For other models that don't satisfy the existence condition, generally, the former lower order modes $L(0, m)$ and $F(1, m)$ ($m \leq 3$) are the dominant modes, which amplitudes are larger than those of the other higher order modes $L(0, m)$ and $F(1, m)$ ($m > 3$), respectively.

The vibration distributions of the normal modes and the Stoneley modes are different. The energies of the normal modes are trapped in the layer which has the smaller shear velocity, while the Stoneley modes are the interfacial waves propagated in the cylindrical interface between the rod and cladding. Moreover, in the case of each lowest branch flexural mode $F(1, 1)$, radial displacement component is always larger than axial displacement component at the same radial distance through the whole radial direction cross-section.

Both the dispersion characteristics and excitation mechanisms of the guided waves propagated in a rod surrounded by an infinite cladding are studied together in this paper, while further research focusing on the modeling experiments should be undertaken in laboratory in the future.

ACKNOWLEDGMENTS

This work is supported by the National Natural Science Foundation of China under Grant no. 10774158. Hanyin Cui is also grateful to the Newton International Fellowships.

REFERENCES

1. V. Madenga, D. H. Zou, and C. Zhang, J. Appl. Geophys. **59**, 79 (2006).
2. A. Ivanovic, R. D. Neilson, and A. A. Rodger, J. Geotech. Geoenvir. Engrg. **128**, 237 (2002).
3. A. Ivanovic and R. D. Neilson, Int. J. Rock Mech. Mining Sci. **45**, 941 (2008).
4. B. R. Mace and E. Manconi, J. Sound Vib. **318**, 884 (2008).
5. D. C. Gazis, J. Acoust. Soc. Am. **31**, 568 (1959).
6. Y. H. Pao and R. D. Mindlin, J. Appl. Mech. **27**, 513 (1960).
7. W. Sachse and Y. H. Pao, J. Appl. Phys. **49**, 4320(1978).
8. R. Thurston, J. Acoust. Soc. Am. **64**, 1 (1978).
9. J. L. Rose, *Ultrasonic Waves in Solid Media* (Cambridge Univ., Cambridge, 1999).
10. J. Li and J. L. Rose, J. Acoust. Soc. Am. **109**, 457 (2001).
11. J. L. Rose, K. M. Rajana, and M. K. T. Hansch, J. Adhes. **50**, 71 (1995).
12. M. J. S. Lowe, IEEE Trans. UFFC **42**, 525 (1995).
13. B. N. Pavlakovic, M. J. S. Lowe, D. Alleyne, and P. Cawley, Rev. Progr. QNDE **16**, 185 (1997).
14. M. D. Beard, M. J. S. Lowe, and P. Cawley, J. Mater. Civil Eng. **15**, 212 (2003).
15. M. D. Beard and M. J. S. Lowe, Int. J. Rock Mech. Mining Sci. **40**, 527 (2003).
16. B. X. Zhang, H. Y. Cui, B. X. Xiao, and C. G. Zhang, Chin. Phys. Lett. **24**, 2883 (2007).
17. U. Kawald, C. Desmet, W. Lauriks, C. Glorieux, and J. Thoen, J. Acoust. Soc. Am. **99**, 926 (1996).
18. M. Kley, C. Valle, L. J. Jacobs, J. Qu, and J. Jarzynski, J. Acoust. Soc. Am. **106**, 582 (1999).
19. A. L. Kurkjian and S. K. Chang, Geophysics **51**, 148 (1986).
20. D. P. Schmitt, J. Acoust. Soc. Am. **84**, 2215(1988).
21. B. X. Zhang, H. F. Dong, and K. X. Wang, J. Acoust. Soc. Am. **96**, 2546 (1994).
22. I. Onda, S. Komaki, and M. Ichikawa, J. Phys. Earth **23**, 205 (1975).
23. B. X. Zhang, M. Yu, C. Q. Lan, and W. Xiong, J. Acoust. Soc. Am. **100**, 3527 (1996).
24. Z. X. Yao, Acta. Geophys. Sinica **22**, 181 (1979).
25. A. H. Meitzler, J. Acoust. Soc. Am. **33**, 435 (1961).
26. R. Stoneley, Proc. R. Soc. London **106**, 416 (1924).
27. A. S. Ginzbarg and E. Strick, Bull. Seismol. Soc. Am. **48**, 51 (1958).